Available online at www.sciencedirect.com

ScienceDirect

Proceedings of the Combustion Institute 36 (2017) 1967–1975

Proceedings of the Combustion Institute

www.elsevier.com/locate/proci

The cross-scale physical-space transfer of kinetic energy in turbulent premixed flames

Jeffrey O'Brien [a], Colin A.Z. Towery [b], Peter E. Hamlington [b], Matthias Ihme [a], Alexei Y. Poludnenko [c], Javier Urzay [a,*]

[a] *Center for Turbulence Research, Stanford University, Stanford, CA 94305-3024, United States*
[b] *Department of Mechanical Engineering, University of Colorado, Boulder, CO 80309, United States*
[c] *Laboratories for Computational Physics and Fluid Dynamics, Naval Research Laboratory, Washington, D.C. 20375, United States*

Received 3 December 2015; accepted 20 May 2016
Available online 25 June 2016

Abstract

Multi-scale interactions and kinetic-energy transfer between turbulence and flames are fundamental to understanding and modeling premixed turbulent reacting flows. In order to investigate these phenomena, direct numerical simulations of a turbulent premixed flame are analyzed in this study. The results reveal a flux of kinetic energy that involves a cross-scale transfer through the turbulence cascade and whose prevailing direction in the flame brush is from subgrid to resolved scales. The root cause of this reversal in energy transfer, termed subgrid-scale (SGS) backscatter, is the effect of thermal expansion in the subgrid scales, by which small amounts of enthalpy created by combustion heat release are transformed into small-scale kinetic energy by means of the SGS pressure-gradient velocity correlation. The resulting overload of SGS kinetic energy is transferred to the resolved scales through SGS backscatter. This cross-scale flux of energy, along with a larger one that relies on large-scale quantities only and does not involve the energy cascade, describes the transformation of combustion heat release into kinetic energy in the turbulent premixed flame. Based on scaling analyses, it is theorized that the contribution of the cross-scale flux to the total kinetic-energy augmentation vanishes in combustion regimes in which the flame-transit time is too short to allow for activation of the non-linear convective mechanisms of the energy cascade.

Keywords: Turbulent premixed flames; Direct numerical simulations; Subgrid-scale modeling

1. Introduction

The heat released from combustion chemical reactions leads to thermal expansion in premixed flames, and, as a result, to hydrodynamic coupling with the turbulent gas environment. The resulting

* Corresponding author.
E-mail address: jurzay@stanford.edu (J. Urzay).

http://dx.doi.org/10.1016/j.proci.2016.05.005
1540-7489 © 2016 by The Combustion Institute. Published by Elsevier Inc.

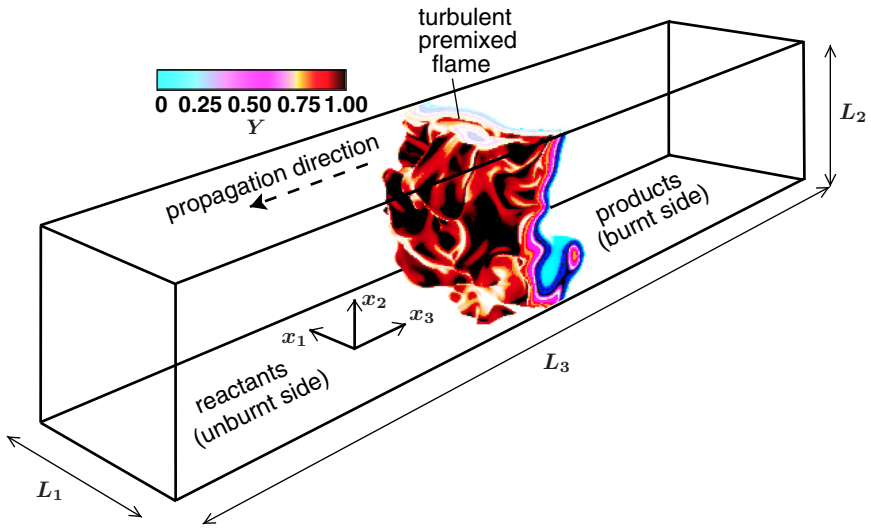

Fig. 1. Schematics of the computational setup, including a DNS snapshot of the turbulent deflagration showing isocontours of the fuel mass fraction Y.

inhomogeneous and anisotropic density variations influence the transport of mass, momentum and energy. However influential these effects may be for commanding exchanges between kinetic and thermal energies across multiple scales, the extent to which combustion-driven thermal expansion modifies the classical picture of the direct energy cascade is largely unknown. On the contrary, standard descriptions of turbulence-flame interactions make use of Kolmogorov's equilibrium concepts [1]. Studies of these effects are of practical interest for developing predictive large-eddy simulation (LES) capabilities for turbulent flames.

Most LES closure models for turbulent transport have been designed for non-reacting flows, and are known to concur with the direct energy cascade whereby a balance between dissipation and production (or forward transfer of energy from resolved scales) is satisfied in the subgrid. The occurrence of inertial transfer of kinetic energy from the subgrid to the resolved scales is classically referred to as subgrid-scale (SGS) backscatter [2–5]. However, this reverse transfer of energy leads to unphysical eddy-viscosity coefficients [4]. In incompressible homogeneous-isotropic turbulence (HIT), the flux of kinetic energy across the cascade is known to be directed from the resolved to the subgrid scales in the mean, with excursions in the opposite backscattering direction being frequently observed due to intermittency [5,6]. In contrast, in the combustion regime analyzed here, it is shown below that kinetic energy is transferred from subgrid to resolved scales on average rather than sporadically.

The problem addressed computationally in this study is a premixed flame propagating in HIT along a prismatic unconfined domain with periodic boundary conditions in the transverse directions, as depicted in Fig. 1. Focus is placed on quantifying the cross-scale transfer of kinetic energy, defined here as the flux between subgrid and resolved scales across the cutoff imposed by a low-pass filter. Before describing the numerical results, an analysis of characteristic scales is performed in the next section to ascertain under which conditions kinetic-energy transfer across the turbulence cascade is relevant in premixed flames.

2. Characteristic scales associated with the transfer of kinetic energy in premixed flames

The heat released in laminar planar premixed flames produces a gasdynamic pressure decrease ΔP across the flame thickness δ_L that is proportional to the square of the flame speed S_L. The pressure variation can be computed from the Rankine–Hugoniot relations as $\Delta P \sim \gamma \mathrm{Ma}^2 \tau P_u/(1-\tau)$, where $\mathrm{Ma} = S_\mathrm{L}/(\gamma P_u/\rho_u)^{1/2}$ is the Mach number, which is small in weak deflagrations far from the lower Chapman–Jouget conditions. Additionally, ρ_u and P_u are the unburnt density and pressure, γ is the adiabatic coefficient, and $\tau = (T_b - T_u)/T_b$, is the heat-release or thermal-expansion coefficient, with T_u and T_b the unburnt and burnt temperatures, respectively. Conservation of momentum across the flame requires ΔP to be balanced with a characteristic increase of kinetic energy per unit mass across the flame given by

$$\Delta k = \frac{(2-\tau)\Delta P}{2(1-\tau)\rho_u} = A S_\mathrm{L}^2 \qquad (1)$$

in the reference frame moving at the flame speed. The dimensionless coefficient $A = (2-\tau)\tau/[2(1-\tau)^2] \gg 1$ is of order 30–40 in practical applications, which indicates that the relative increase in kinetic energy can be several times the square of the laminar flame speed. In the laboratory frame, the increase in kinetic energy is of the same order as (1), with $[\tau/4(1-\tau)]^2$ replacing A.

In turbulent premixed flames, the simple description given above is incomplete due to multi-scale interactions [7,8]. As with laminar flames, only a small portion of the heat released in the flame is transformed into kinetic energy. However, both mean and fluctuating kinetic energies are influenced by combustion. The most important effect of heat release is the augmentation of the mean kinetic energy, corresponding to the large scales of the flow. This mean transfer of energy does not require a cascade mechanism, as it transforms large-scale thermal enthalpy into large-scale kinetic energy through the work done by the large-scale pressure gradient. As the turbulent eddies move through the flame, however, they become subjected to the multi-scale anisotropic action of heat release, which distorts their shape and fluctuating kinetic energies [9].

The propagation of thermal distortions caused by combustion heat release across the turbulence kinetic-energy cascade takes place over a characteristic transfer time. In incompressible turbulent flows, a model for the characteristic transfer time across the cascade was proposed by Lumley [10], whereby the time required for energy to cascade from large to small scales is of the same order as the large-scale eddy turnover time $t_\ell \sim \ell/u_\ell$, where ℓ is the integral length and u_ℓ the corresponding velocity. Using this estimate, for the cascade transfer of energy to take place within the flame brush, the propagation time t_ℓ must be smaller than the characteristic flame-transit time, $t_L \sim \delta_L/S_L$, with the Damköhler number $\mathrm{Da} = t_\ell/t_L$ measuring their ratio. However, not all combustion regimes satisfy this condition, as shown in Fig. 2.

The condition $t_\ell \lesssim t_L$ is unachievable in weakly turbulent flames, which are characterized by $u_\ell/S_L \ll 1$ and $\mathrm{Da} \gg 1$. In these, the mean flow is too fast to allow for activation of transfer across the cascade in the flame. In this limit, the flame thickness $\delta_L < \ell_k$ is in the dissipative range of the turbulence according to the high Reynolds numbers involved, $\mathrm{Re}_\ell = u_\ell \ell/\nu \gg 1$, with ℓ_k the Kolmogorov length and ν the kinematic viscosity. In this way, any cascade interaction through convective transport between small and large scales is relegated to the far wake of the burnt gases, at downstream distances of order $\ell S_L/u_\ell \gg \ell$. This spatial delay is the result of the rapid distortion involved in the passage of turbulence through the thin wrinkled flame, whose analytical description does not require to retain non-linear convective terms in the first approximation [11].

At moderate turbulent intensities $u_\ell/S_L \sim A^{1/2} > 1$ the characteristic energy increase (1) becomes of the same order as the turbulent kinetic energy, $\Delta k/u_\ell^2 \sim 1$. The interaction departs from the rapid-distortion dynamics described above as the flame-transit time becomes comparable to inertial time scales, $\mathrm{Da} \sim 1$. These values of u_ℓ/S_L and Da involve flame thicknesses of order $\delta_L \sim \ell A^{-1/2} < \ell$ corresponding to spatial scales in the inertial subrange, with Karlovitz numbers of order $\mathrm{Ka} = (u_\ell/S_L)^{3/2}(\delta_L/\ell)^{1/2} \sim A^{1/2} > 1$. In this limit, the residence time of the large eddies in the flame is sufficiently long to enable transfer of energy across the entire range of scales of the cascade in the flame brush. The corresponding combustion regime corresponds to the thin-reaction zones.

Too large departures from the conditions $\mathrm{Da} \sim 1$ and $u_\ell/S_L \sim A^{1/2}$ diminish the importance of energy transfer through the cascade mechanism. For instance, while small values of the turbulent intensity render too short times for transport across the cascade, too large intensities $u_\ell/S_L \gg A^{1/2}$ imply $\Delta k/u_\ell^2 \ll 1$, which leads to very weak thermal distortions of the highly energetic turbulence. Similarly, smaller Damköhler numbers imply larger residence times for eddies in the flame brush, but also rapidly decaying turbulence unless external forcing is applied. As the Damköhler number increases above unity when $u_\ell/S_L > A^{1/2}$, it becomes less likely for the large scales in the flame brush to receive or give energy to the small scales. However, in these conditions, energy transfer through the cascade is active in the flame brush across an interval of smaller scales formed by $\ell_m \sim \delta_L u_m/S_L$ and ℓ_k, with ℓ_m the scale at which the eddy turnover time is of the same order as the flame-transit time, with $\mathrm{Da}_m = \ell_m/(u_m t_L) \sim 1$ the associated Damköhler number. In this regime, for LES cutoffs $\Delta > \ell_m$ the energy cascade is necessarily confined to subgrid scales.

In this phenomenological description, no mention has been made of the direction of the cascade when it is active in the flame brush, whether the energy transfer is from resolved to subgrid scales or vice-versa, although the computations shown below suggest that the energy is predominantly transferred from small to large scales. Similarly, the turbulence energy cascade is readily conceptualized in Fourier space in incompressible HIT. However, the inhomogeneity of the streamwise direction, along with variations of density and molecular diffusivities, complicates spectral analyses in premixed flames. Low-pass filtering the conservation equations, as done below, does not require any periodicity and provides three-dimensional fluxes across the filter scale that originate from cumulative non-linear convective interactions responsible for the cascade [2]. The spectral representation of these cross-scale fluxes in sums of triadic ones is straightforward in incompressible HIT [12], but not in pre-

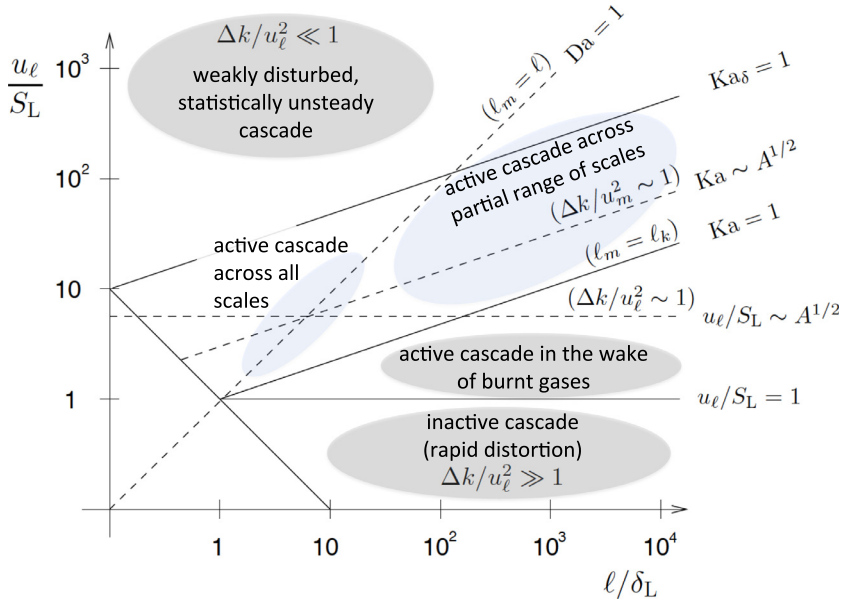

Fig. 2. Combustion regime diagram [1] adapted to highlight the turbulence-cascade characteristics in the flame brush.

mixed flames. The analysis below is therefore precluded to physical-space considerations.

3. Formulation and computational setup

In this study, the unsteady, compressible, chemically-reacting Navier–Stokes equations

$$\begin{aligned}
&\frac{\partial \rho}{\partial t} + \frac{\partial}{\partial x_i}(\rho u_i) = 0,\\
&\frac{\partial}{\partial t}(\rho u_i) + \frac{\partial}{\partial x_j}(\rho u_i u_j) = -\frac{\partial P}{\partial x_i} + \frac{\partial \tau_{ij}}{\partial x_j} + \rho F_i,\\
&\frac{\partial}{\partial t}(\rho Y) + \frac{\partial}{\partial x_j}(\rho u_j Y) = \frac{\partial}{\partial x_j}\left(\rho D \frac{\partial Y}{\partial x_j}\right) - \rho \dot{w},\\
&\frac{\partial}{\partial t}(\rho e_t) + \frac{\partial}{\partial x_j}(\rho u_j e_t) = -\frac{\partial}{\partial x_j}(P u_j)\\
&\quad + \frac{\partial}{\partial x_j}(\tau_{ij} u_i) + \frac{\partial}{\partial x_j}\left(\kappa \frac{\partial T}{\partial x_j}\right) + \rho q \dot{w}, \qquad (2)
\end{aligned}$$

are integrated numerically along with the equation of state $P = \rho R_g T$. In this formulation, ρ is the density, u_i are the velocity components, P is the thermodynamic pressure, T is the temperature, F_i is a volumetric forcing term, e_t is the total energy (including thermal and kinetic energies), Y is the fuel mass fraction, R_g is the gas constant, and κ and D are the thermal conductivity and mass diffusivity, respectively. Additionally, $\tau_{ij} = 2\mu S_{ij} + \eta \Delta_v \delta_{ij}$ is the viscous stress tensor, with μ being the dynamic viscosity, η the second viscosity coefficient ($\eta = \mu$ is used here), $\Delta_v = S_{ii}$ the flow dilatation, and $S_{ij} = (1/2)(\partial u_i/\partial x_j + \partial u_j/\partial x_i)$ the strain-rate tensor. Constant specific heats are used in the calculations, while temperature-dependent values of viscosity, thermal conductivity and mass diffusivity are employed according to a power law with exponent 0.7.

The computations are performed using Athena-RFX [13]. The flame propagation regime studied pertains to low Mach numbers. However, the thermodynamic pressure gradient, kinetic energy and viscous dissipation are retained in writing Eq. (2) because the numerical scheme is compressible. It consists of a fully unsplit, finite-volume, Godunov-type integration algorithm [14] that accounts for molecular fluxes and utilizes a PPM-type spatial reconstruction along with a HLLC Riemann solver.

A single-step irreversible Arrhenius reaction between fuel and oxidizer is assumed in which the former is the limiting reactant, with q units of heat being released per unit mass of fuel burnt. The corresponding chemical source in (2) is $\dot{w} = \rho B Y \exp(-T_a/T)$ in terms of an activation temperature T_a and a pre-exponential factor B. In the following, use of the progress variable $C = 1 - Y$ is made, with $C = 0$ on the reactants side while $C = 1$ on the products side.

The computations are carried out on a uniform Cartesian grid of $512 \times 512 \times 16,384$ elements in the x_1, x_2 and x_3 directions, respectively. The corresponding domain lengths are $L_1/\delta_L = L_2/\delta_L = 8$ and $L_3/\delta_L = 256$ (see Fig. 1), which provide 4.2 and 134 integral lengths in the spanwise and streamwise directions, respectively. The minimum grid spacing h satisfies $\delta_L/h = 64$ and $\ell/h = 122$, as well as $\ell_k/h = 2$ and $\ell_k/h = 25$ on the reactants and products sides, respectively, with the effective resolution increasing in the burnt gases as a result of a 27-fold increase in ν with temperature. Periodic boundary

conditions are used in the x_1 and x_2 directions. The boundaries in the x_3 direction are periodic prior to ignition of the premixed flame, while zero-order extrapolation boundary conditions are used after ignition in order to allow gases to flow in and out without causing a build-up of pressure.

The simulations are initialized as follows. First, in absence of combustion, forced turbulence is let to develop everywhere in the computational domain for a duration of $6t_\ell$. The forcing F_i, which only acts upon the largest scales and whose details can be found elsewhere [13], remains active for the remainder of the simulation in order to enable the calculation of steady statistics. After this spin-up phase, a planar laminar flame is inserted in the domain and is allowed to develop for another $6t_\ell$, during which transition to a fully turbulent reacting regime occurs, with 27 three-dimensional solution snapshots recorded thereon during $3t_\ell$. Ensemble-averaged statistics, denoted by the symbol $\langle\cdot\rangle_N$, are computed from these snapshots after planar-averaging the relevant variables, the latter being represented by the operator $\langle\cdot\rangle$ corresponding to spatial averaging over the transverse planes $\{x_1, x_2\}$.

Turbulence-flame interactions are characterized by $u_\ell/S_\mathrm{L} = 2.7$, $\mathrm{Re}_\lambda = 86.5$ (with λ the Taylor scale), $\mathrm{Da} = 0.71$, $\mathrm{Ka} = 20.7$, $\tau = 0.87$ ($A = 29.1$), $\tau T_a/T_b = 5.7$ and $\mathrm{Ma} = 0.01$, while a unity Lewis number is employed for the reactant. In this range of parameters, the flame corrugation caused by turbulence increases the global fuel consumption speed up to factors of order 4 relative to S_L. The resulting values of these dimensionless parameters may be ascribed to the thin-reaction zones, with $\delta_\mathrm{L} = 0.52\ell$ in the inertial subrange. However, the release of chemical energy increases the products temperature by a factor of 7, which leads to a 28-fold increase in the kinematic viscosity on the burnt side of the flame. This effect, in turn, drastically reduces the value of the Reynolds number on the products side. As a result, no significant flame broadening is observed, as shown in Fig. 3.

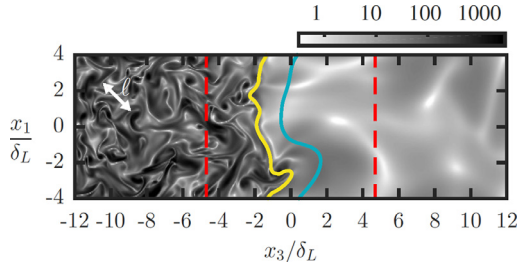

Fig. 3. Instantaneous mid-plane DNS field of enstrophy normalized by $(S_\mathrm{L}/\delta_\mathrm{L})^2$ at $t = 14.1t_\ell$. The white line with arrowheads indicates the integral length ℓ. Yellow and blue lines represent, respectively, $C = 0.05$ and $C = 0.95$, while red-dashed lines indicate the boundaries of the interval $0.005 < \langle C\rangle < 0.995$. (For interpretation of the references to color in this figure legend, the reader is referred to the web version of this article.)

4. Kinetic-energy transfer dynamics

In order to calculate the cross-scale transfer of kinetic energy between resolved and subgrid levels, a differential filter [15] is applied to the DNS velocity, which results in resolved eddy motion whose kinetic energy is $k = \widetilde{u}_i\widetilde{u}_i/2$. In the notation, overlines and tildes denote regular and Favre filtering, respectively. In the results shown below, the filter width is varied from $\Delta = \delta_\mathrm{L}/4$ to $\Delta = 4\delta_\mathrm{L}$. The difference between the filtered kinetic energy of the full-scale flow field, $\widetilde{K} = \widetilde{u_i u_i}/2$, and the resolved kinetic energy, k, corresponds to the SGS kinetic energy, $k_\mathrm{SGS} = (\widetilde{u_i u_i} - \widetilde{u}_i\widetilde{u}_i)/2$.

A transport equation for the resolved kinetic energy is obtained by filtering the momentum equation in (2) and multiplying it by $\widetilde{u}_i$, which yields the expression

$$\frac{\partial k}{\partial t} + \widetilde{u}_i\frac{\partial k}{\partial x_i} = \alpha_p + \alpha_v + \alpha_\mathrm{SGS} + f. \tag{3}$$

In this formulation, α_p, α_v and α_SGS are given by

$$\overline{\rho}\alpha_p = -\widetilde{u}_i\frac{\partial \overline{P}}{\partial x_i}, \quad \overline{\rho}\alpha_v = \widetilde{u}_i\frac{\partial \overline{\tau}_{ij}}{\partial x_j}, \quad \overline{\rho}\alpha_\mathrm{SGS} = -\widetilde{u}_i\frac{\partial \mathcal{T}_{ij}}{\partial x_j}, \tag{4}$$

which represent the work done by the resolved pressure, resolved viscous stresses and unresolved turbulent stresses, respectively. In Eq. (4), $\mathcal{T}_{ij} = \overline{\rho}(\widetilde{u_i u_j} - \widetilde{u}_i\widetilde{u}_j)$ is the SGS stress tensor, and $f = \widetilde{F_i u_i}$ is the resolved energy injected by the forcing.

Subtraction of (3) from the transport equation of $\widetilde{K}$, obtained by multiplying the momentum equation in (2) by u_i and filtering the corresponding expression, leads to the transport equation

$$\frac{\partial k_\mathrm{SGS}}{\partial t} + \widetilde{u}_i\frac{\partial k_\mathrm{SGS}}{\partial x_i} = \alpha_p^\mathrm{SGS} - \alpha_\mathrm{SGS} + \alpha_v^\mathrm{SGS} + \phi_\mathrm{SGS} + f_\mathrm{SGS}, \tag{5}$$

where

$$\overline{\rho}\alpha_p^\mathrm{SGS} = \widetilde{u}_i\frac{\partial \overline{P}}{\partial x_i} - \overline{u_i\frac{\partial P}{\partial x_i}} \tag{6}$$

is the SGS pressure-gradient velocity correlation (in analogy to Reynolds-Averaged Navier Stokes RANS terminology [17]), and

$$\overline{\rho}\alpha_v^\mathrm{SGS} = \overline{u_i\frac{\partial \tau_{ij}}{\partial x_i}} - \widetilde{u}_i\frac{\partial \overline{\tau}_{ij}}{\partial x_i} \tag{7}$$

is the SGS viscous work. Additionally,

$$\overline{\rho}\phi_\mathrm{SGS} = -\frac{\partial}{\partial x_i}\left(\overline{\rho}\widetilde{u_i K} - \overline{\rho}\widetilde{u}_i\widetilde{K}\right) \tag{8}$$

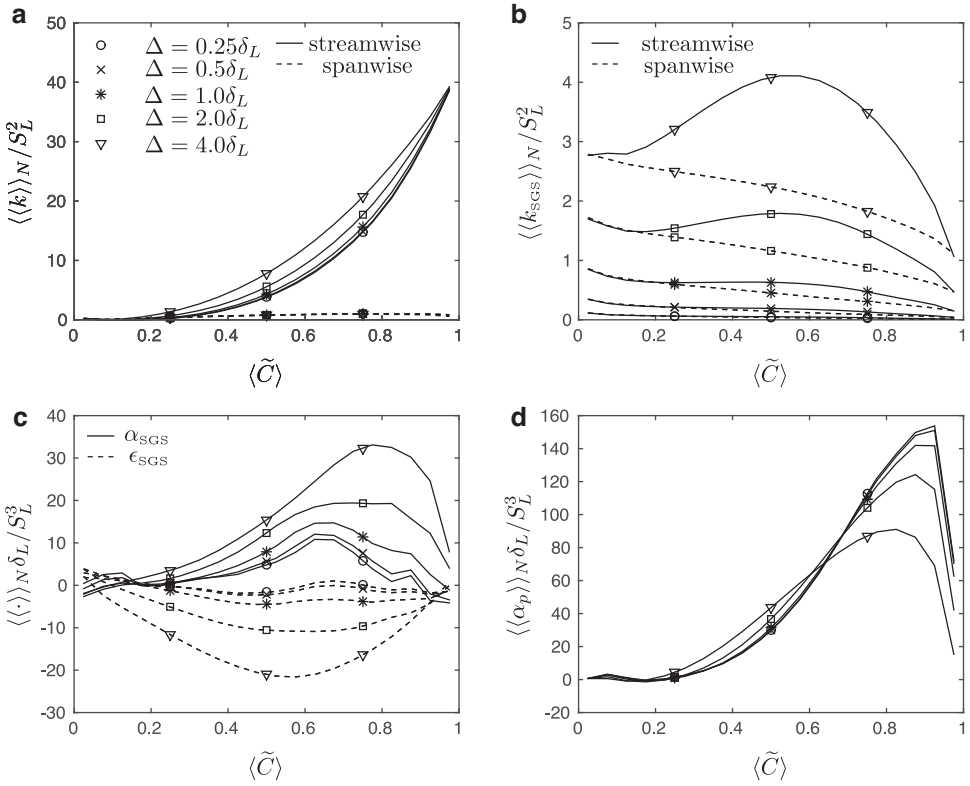

Fig. 4. Ensemble-planar-averaged distributions conditioned on the planar-averaged progress variable for (a) resolved and (b) subgrid kinetic energies, including streamwise and spanwise components, along with (c) SGS and (d) pressure-gradient transport in the budget of resolved kinetic energy (3).

is an unclosed flux of the full-scale kinetic energy that contains a filtered triple product of velocities. The term $f_{SGS} = \widetilde{F_i u_i} - \widetilde{F_i}\widetilde{u_i}$ corresponds to external forcing energy injected in the subgrid, which is negligible since F_i acts primarily upon the largest scales.

The SGS flux α_{SGS}, defined in (4), appears on the right hand sides of both transport Eqs. (3) and (5), thereby indicating a two-way connection between the resolved and subgrid energetics. In conservative form, it can be written as $\overline{\rho}\alpha_{SGS} = -\partial(\mathcal{T}_{ij}\widetilde{u_i})/\partial x_j - \overline{\rho}\epsilon_{SGS}$, where $\overline{\rho}\epsilon_{SGS} = -\mathcal{T}_{ij}\widetilde{S}_{ij}$ is the SGS dissipation and $\widetilde{S}_{ij}$ is the strain rate of the resolved velocity field. In incompressible HIT, ϵ_{SGS} is the prevailing mechanism for transfer of kinetic energy between resolved and subgrid scales [5,6,12], with $\rho\langle\epsilon_{SGS}\rangle = \langle\overline{\tau_{ij}S_{ij}} - \overline{\tau_{ij}}\widetilde{S}_{ij}\rangle$ indicating the subgrid production–dissipation average balance implicitly assumed in LES modeling strategies. In particular, $\epsilon_{SGS} < 0$ corresponds to an intermittent reverse flux of kinetic energy from subgrid to resolved scales that has been referred to as SGS backscatter [2–5]. In the present configuration, however, SGS backscatter is more expediently indicated by $\alpha_{SGS} > 0$ due to the streamwise inhomogeneity caused by thermal expansion in the premixed flame.

The resolved kinetic energy k increases through the flame brush, as shown in Fig. 4(a). There are two sources of augmentation of k in (3) acting through different paths: the resolved pressure-gradient work $\alpha_p > 0$, resulting directly from the large-scale density gradient across the flame, and the transfer of energy from subgrid to resolved scales given by $\alpha_{SGS} > 0$. The relative strength of both sources can be inferred from Fig. 4(c,d), which shows that $\alpha_{SGS} < \alpha_p$, suggesting that most of the production of large-scale kinetic energy (approx. 80% for $\Delta = 2\delta_L$) does not involve transfer across the cascade. The remainder is produced by a cross-scale transfer or SGS backscatter of energy from subgrid to resolved scales.

The SGS kinetic energy k_{SGS} increases across the flame, as shown in Fig. 4(b). Nonetheless, the increase of viscosity on the products side, which leads to a 6-fold decrease in Re_λ, rapidly attenuates the upsurge of k_{SGS}, as evidenced by the globally decaying trend in Fig. 4(b). The increase in k_{SGS} is observed to produce, on average, a prevailing SGS backscatter that enables the transfer of the

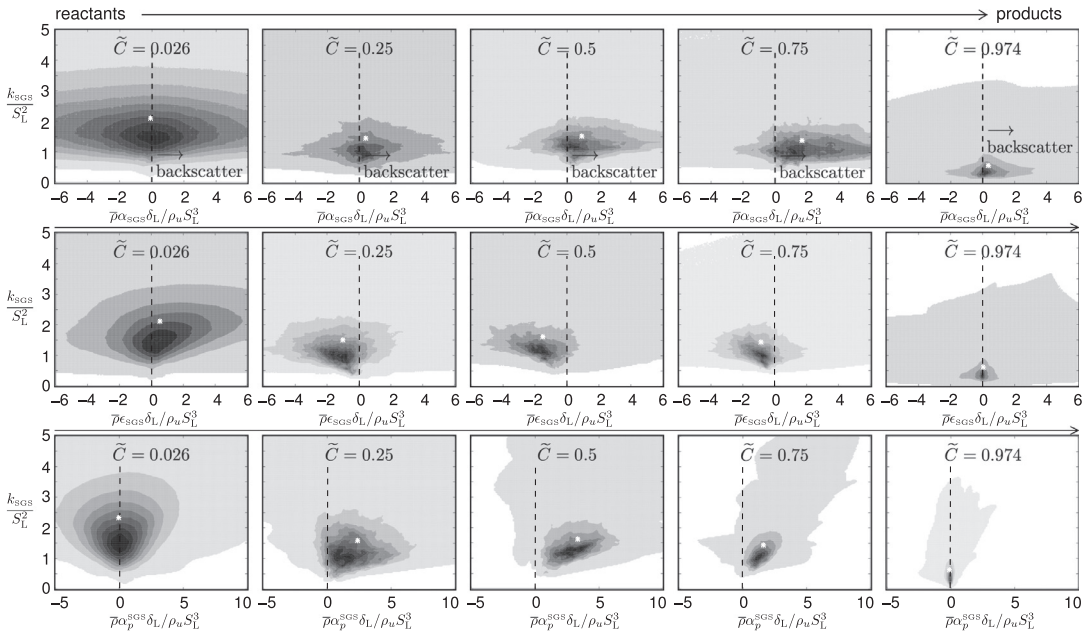

Fig. 5. Normalized joint probability density functions conditioned on the local Favre-filtered progress variable for SGS kinetic energy versus: SGS production rate (upper row), SGS dissipation (center row) and SGS pressure-gradient velocity correlation (bottom row), all panels being computed for $\Delta = 1.0\delta_L$. The white dots represent global averages.

excess SGS kinetic energy toward resolved scales. This phenomenon is shown in Fig. 4(c), where the ensemble-planar-averaged α_{SGS} varies from being negative in the upstream HIT (indicating the usual mean transfer from resolved to subgrid scales), to being positive in the flame (indicating transfer from subgrid to resolved scales) and decreasing downstream as a result of the much lower turbulent intensity there. Statistics of this process, conditioned on the local (rather than planar-averaged) progress variable, are shown in the upper row of Fig. 5 in terms of the joint PDFs between k_{SGS} and $\overline{\rho}\alpha_{SGS}$. Specifically, while upstream from the flame no clear pattern of joint dynamics is discerned, SGS backscatter becomes statistically dominant in the flame. Similar conclusions are obtained for the SGS dissipation in the center row, where it is observed that the statistics strongly differ from the mean forward-dissipating dynamics in incompressible HIT [5,6]. It is noteworthy that, in contrast to non-premixed combustion in mixing layers studied in [16], where it was found that a net forward-scatter of energy occurred in the mean across the mixing layer, in the present study a net backscatter is obtained on average in the premixed-flame brush.

The main source of k_{SGS} is the effect of thermal expansion in the subgrid, or equivalently the SGS pressure-gradient velocity correlation α_p^{SGS}, as shown in Fig. 6(a). The joint staistics of $\overline{\rho}\alpha_p^{SGS}$ and k_{SGS} are depicted in the bottom row in Fig. 5. In particular, a clear correlation trend between the two arises in the flame, with correlation coefficient 0.90 at $\widetilde{C} = 0.75$. The clear energy imbalance created by α_p^{SGS} in the subgrid suggests that additional modeling considerations may be needed for turbulent transport models based on (5). Furthermore, the results shown in Fig. 6(b) suggest that the SGS transport flux to higher moments ϕ_{SGS} also participates in the local transfer of k_{SGS}, although its net contribution integrated across the flame is much smaller than that of α_p^{SGS}. In particular, ϕ_{SGS} displays an oscillatory trend whose sign is exactly the opposite of the curvature of the k_{SGS} profile, which suggests that a negative eddy viscosity would be required if ϕ_{SGS} were modeled using a gradient assumption in analogy to RANS [17]. Since such an eddy viscosity would render the solution unstable, it is evident that a different model form is required to account for the additional thermal-expansion phenomena.

5. Concluding remarks

The energy-transfer dynamics described in this study can be summarized in the flux diagram shown in Fig. 7. The results reveal the occurrence of a flux of kinetic energy that involves a cross-scale transfer through the turbulence cascade and whose prevailing direction in the flame is from subgrid to resolved scales. The root cause of this reverse trans-

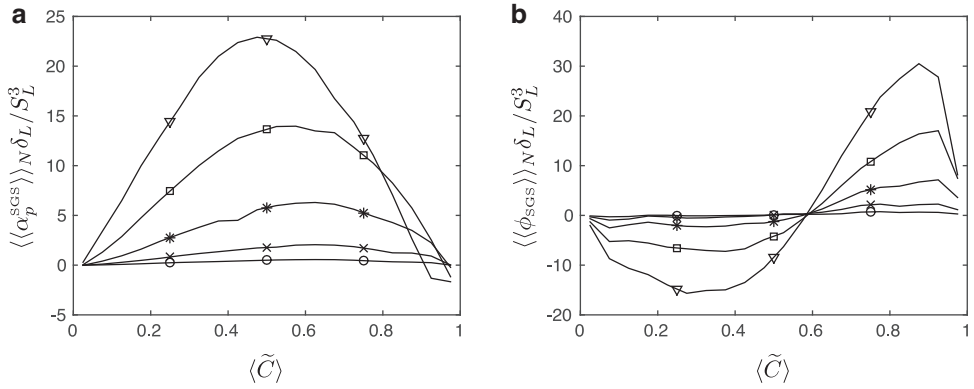

Fig. 6. Ensemble-planar-averaged distributions conditioned on the planar-averaged progress variable for (a) SGS pressure-gradient velocity correlation and (b) SGS transport flux in the budget of SGS kinetic energy (5) (see legend in Fig. 4(a)).

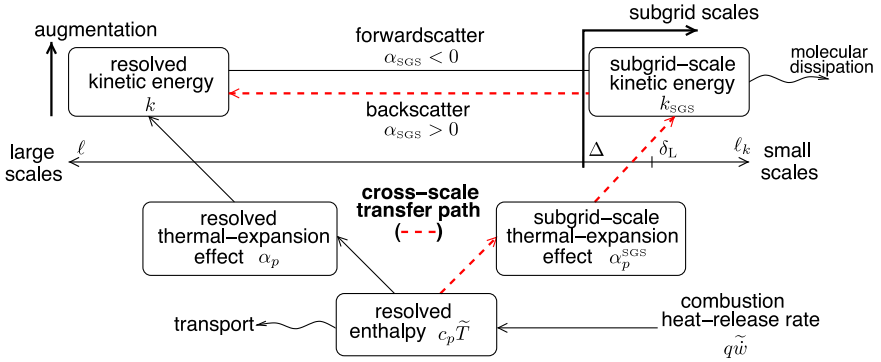

Fig. 7. Schematic of kinetic-energy transfer pathways in premixed flames.

fer is the effect of thermal expansion in the subgrid, which is manifested in the form of a SGS pressure-gradient velocity correlation that transforms small amounts of enthalpy created by the combustion heat into SGS kinetic energy. The excess of SGS kinetic energy is transferred to the resolved scales by SGS backscatter. Scaling analyses suggest that the contribution of the cross-scale flux to the total kinetic-energy augmentation vanishes in combustion regimes in which the flame-transit time is too short to allow for activation of the non-linear convective mechanisms of the energy cascade.

In connection with the results presented here, Fourier analyses of turbulent premixed flames have pointed out similarly relevant effects of the pressure-gradient work at small scales on the kinetic-energy spectrum [7] and have addressed the occurrence of spectral backscatter in the flame [8]. An aspect worthy of further research is the effect that the observed breakdown of equilibrium in the subgrid has on the turbulent fluxes across the flame, including possible relations with the unsolved problem of SGS counter-gradient transport [18].

Acknowledgments

This investigation was funded by the US AFOSR Grants # FA9550-14-1-0219 and FA9550-14-1-0273 monitored by Dr. Chiping Li.

References

[1] N. Peters, *Turbulent Combustion*, Cambridge Univ. Press, 2000.
[2] D.C. Leslie, G.L. Quarini, *J. Fluid Mech.* 91 (1976) 65–91.
[3] U. Piomelli, W. Cabot, P. Moin, S. Lee, *Phys. Fluids* 3 (1991) 1766–1771.
[4] J.A. Domaradzki, E.M. Saiki, *Theor. Comp. Fluid Dyn.* 9 (1997) 75–83.
[5] T. Ishihara, T. Gotoh, Y. Kaneda, *Annu. Rev. Fluid Mech.* 41 (2009) 165–180.
[6] J.I. Cardesa, A. Vela-Martín, S. Dong, J. Jiménez, *Phys.Fluids* 27 (2015) 111702.
[7] H. Kolla, E.R. Hawkes, A.R. Kerstein, N. Swaminathan, J.H. Chen, *J. Fluid Mech.* 754 (2014) 456–487.
[8] C.A.Z. Towery, A.Y. Poludnenko, J. Urzay, J. O'Brien, M. Ihme, P.E. Hamlington, *Phys. Rev.* E 93 (2016) 053115.

[9] P.E. Hamlington, A.Y. Poludnenko, E.S. Oran, *Phys.Fluids* 23 (2015) 125111.
[10] J.L. Lumley, *Phys. Fluids* 4 (1992) 203–211.
[11] R.C. Aldredge, F.A. Williams, *J. Fluid Mech.* 228 (1991) 487–511.
[12] S.B. Pope, *Turbulent Flows*, Cambridge Univ. Press, 2000.
[13] A.Y. Poludnenko, E.S. Oran, *Combust. Flame* 157 (2010) 995–1011.
[14] J. Saltzman, *J. Comput. Phys.* 115 (1994) 153–168.
[15] M. Germano, *Phys. Fluids* 29 (1986) 1755–1757.
[16] J. O'Brien, J. Urzay, M. Ihme, P. Moin, A. Saghafian, *J. Fluid Mech.* 743 (2014) 554–584.
[17] C.G. Speziale, *Annu. Rev. Fluid Mech.* 23 (1991) 107–157.
[18] F.A. Williams, P.A. Libby, *AIAA Paper* (1980) 80–0012.